EBioMedicine 48 (2019) 592–604

Contents lists available at ScienceDirect

EBioMedicine

journal homepage: www.elsevier.com/locate/ebiom

EBioMedicine
Published by THE LANCET

Age, lipofuscin and melanin oxidation affect fundus near-infrared autofluorescence

Tatjana Taubitz[a,*], Yuan Fang[a], Antje Biesemeier[a,b], Sylvie Julien-Schraermeyer[a], Ulrich Schraermeyer[a,c]

[a] Division of Experimental Vitreoretinal Surgery, Centre for Ophthalmology, University of Tübingen, Schleichstrasse 12/1, 72076 Tübingen, Germany
[b] NMI Natural and Medical Sciences Institute at the University of Tübingen, Reutlingen, Germany
[c] STZ OcuTox Preclinical Drug Assessment, Hechingen, Germany

ARTICLE INFO

Article history:
Received 23 July 2019
Revised 16 September 2019
Accepted 17 September 2019
Available online 21 October 2019

Keywords:
Melanin
Lipofuscin
Melanolipofuscin
Oxidative stress
Aging

ABSTRACT

Background: Fundus autofluorescence is a non-invasive imaging technique in ophthalmology. Conventionally, short-wavelength autofluorescence (SW-AF) is used for detection of lipofuscin, a byproduct of the visual cycle which accumulates with age or disease in the retinal pigment epithelium (RPE). Furthermore, near-infrared autofluorescence (NIR-AF) is used as a marker for RPE and choroidal melanin, but contribution of lipofuscin to the NIR-AF signal is unclear.

Methods: We employed fluorescence microscopy to investigate NIR-AF properties of melanosomes, lipofuscin and melanolipofuscin granules in histologic sections of wildtype and *Abca4*$^{-/-}$ mouse eyes, the latter having increased lipofuscin, as well as aged human donor eyes. Differentiation between these pigments was verified by analytical electron microscopy. To investigate the influence of oxidative and photic stress we used an *in vitro* model with isolated ocular melanosomes and an *in vivo* phototoxicity mouse model.

Findings: We show that NIR-AF is not an intrinsic property of melanin, but rather increases with age and after photic or oxidative stress in mice and isolated melanosomes. Furthermore, when lipofuscin levels are high, lipofuscin granules also show NIR-AF, as confirmed by correlative fluorescence and electron microscopy in human tissue. However, lipofuscin in albino *Abca4*$^{-/-}$ mice lacks NIR-AF signals.

Interpretation: We suggest that NIR-AF is derived from melanin degradation products that accumulate with time in lipofuscin granules. These findings can help to improve the interpretation of patient fundus autofluorescence data.

Funding: This work was supported by Bundesministerium für Bildung und Forschung, Deutsche Forschungsgemeinschaft and Chinese Scholarship Council. Major instrumentation used in this work was supported by Deutsche Forschungsgemeinschaft, the European Fund for Regional Development and the state of Baden-Württemberg.

Research in context

Evidence before this study

Conventional fundus autofluorescence using short-wavelength light for excitation is routinely used for disease monitoring and diagnosis in ophthalmology and its origin from lipofuscin, a pigment in the retinal pigment epithelium, is well established. A further fundus autofluorescence modality employing near-infrared light for excitation is becoming more established in clinical practice, however, the subcellular origin of this signal is not completely understood yet. While it has been established that melanin, both from the retinal pigment epithelium and the choroid, adds to the near-infrared autofluorescence signal, the contribution of lipofuscin to this signal is still disputed.

Added value of this study

With this proof-of-concept study we present two major findings: 1) Near infrared autofluorescence of individual melanosomes increases with age and due to photic and oxidative stress. This im-

* Corresponding author.
E-mail address: tatjana.taubitz@med.uni-tuebingen.de (T. Taubitz).

https://doi.org/10.1016/j.ebiom.2019.09.048

plies that near infrared autofluorescence is not an intrinsic property of melanin but is rather caused by autofluorescent melanin degradation products. 2) Near-infrared autofluorescence can be emitted from individual lipofuscin granules. However, this phenomenon was prevalent in aged tissue with high amounts of lipofuscin granules while it was mostly absent in younger tissue with low amounts of lipofuscin granules.

Implications of all the available evidence

So far, patient near-infrared fundus autofluorescence data were often directly equated with melanin content. Both major findings, near-infrared autofluorescence from melanin increasing with age and oxidative status, as well as lipofuscin being a source of near-infrared autofluorescence under certain circumstances, can help to refine the interpretation of patient near-infrared fundus autofluorescence data. This offers the possibility to gain deeper insights into pathologic processes and refinement of diagnostics for a variety of retinal diseases.

1. Introduction

Melanin is a known anti-oxidant and its cell-protective properties against photic and oxidative injury in the eye are well investigated (reviewed in [1]). However, when melanin ages, the anti-oxidative capability is diminished and is replaced by a pro-oxidative character [2–4]. This transformation is particularly relevant for the retinal pigment epithelium (RPE), a post-mitotic cell layer in the back of the eye. While other pigmented cells in the body, such as skin and choroidal melanocytes, continuously express tyrosinase, the canonical key enzyme of melanogenesis, and therefore are capable to renew their melanin-bearing melanosomes, it is still unknown whether this is also the case for RPE cells (reviewed in [5]). Tyrosinase-independent melanin synthesis in RPE cells was seen *in vitro* [6], but it is unclear whether a substantial melanin-turnover in the RPE exists *in vivo*, making the RPE potentially vulnerable to detrimental effects of aged melanin.

Aging of melanin has been attributed to photodegradation that results in structural modifications such as oxidative cleavage and cross-linking (reviewed in [7]) and is considered to be at least partly responsible for the progression from anti- to pro-oxidative behaviour [8]. During photodegradation of eumelanin, a brown to black type of melanin that is the dominant melanin type in ocular melanosomes, a diaryl ketone product is formed that is highly autofluorescent [9]. Indeed, increased autofluorescence (AF) of biological melanin was found after treatment with light [10–12], hydrogen peroxide [11], superoxide [13], but also as a function of age [14].

Another fluorophore in the RPE is lipofuscin whose key constituent is a class of non-degradable lipids called bisretinoids that emerge as a byproduct of the visual cycle [15]. Due to the (photo-)oxidative properties of some of its components, the accumulation of lipofuscin with age or disease is thought to be associated with RPE dysfunction and subsequent RPE and photoreceptor degeneration [15], but this theory is controversial [16].

In the clinical practice, the importance of investigating fundus AF for the diagnosis and monitoring of retinal disease has increased in recent years. The most common modality is the use of short wavelength AF (SW-AF, excitation 488 nm, emission > 500 nm) to monitor lipofuscin [17]. SW-AF is used in a broad spectrum of retinal diseases, including drug toxicity, inherited retinal dystrophies (such as Stargardt disease, Best macular dystrophy, and retinitis pigmentosa), and age-related macular degeneration [18]. A recent development is the use of near-infrared AF (NIR-AF, excitation 787 nm, emission > 800 nm) that is thought to allow the investigation of ocular melanin [19,20]. NIR-AF investigation has proven to be useful for clinical application, since various ocular diseases, such as age-related macular degeneration [21], Stargardt disease [22], retinitis pigmentosa [23], and others [24] have characteristic changes in NIR-AF patterns that oftentimes precede changes in SW-AF patterns. However, there is still uncertainty whether melanin is the only contributor to NIR-AF, especially lipofuscin is discussed to add to the NIR-AF signal [25].

In this work, we use light, fluorescence and electron microscopy to examine NIR- and SW-AF properties of RPE and choroidal pigment granules of mice, pigs, and humans. Thereby, precise analysis of the contribution of the different pigment types to NIR- and SW-AF signals is facilitated. Furthermore, we investigate whether photic and oxidative damage alters the NIR-AF signal of isolated RPE and choroidal melanosomes, which helps understanding the biological origin and implication of NIR-AF.

2. Materials and methods

2.1. Animals

Pigmented WT mice (129S2), pigmented *Abca4*$^{-/-}$ mice (129S4/SvJae-Abca4^{tm1Ght}) and albino *Abca4*$^{-/-}$ mice (BALB/c-Abca4^{tm1Ght}) were used in this work. WT mice were purchased from Harlan Laboratories (Hillcrest, UK), the knock-out strains were bred in our in-house facility. Light cycling was 12 h light (approximately 50 lx in cages)/12 h dark, food and water were available *ad libitum*. All procedures involving animals were in accordance with the German laws governing the use of experimental animals and were previously approved by the local agency for animal welfare and the local authorities.

2.2. Human donor tissue

Eye globes without known ophthalmic disease were obtained from the cornea bank Tübingen. Written informed consent of the donors for use in medical research and approval of the Institutional Review Board of the University of Tuebingen were obtained. The experiments were performed in adherence to the tenets of the Declaration of Helsinki.

2.3. Blue light damage in mice

Light exposure was performed according to published methods [26] with small modifications. In brief, animals were anesthetized by i.p. injection of a mix of fentanyl (0•05 mg/kg body weight), midazolam (5•0 mg/kg body weight) and medetomidine (0•50 mg/kg body weight). Pupils were dilated with tropicamide drops. Methocel 2% (Omnivision, Puchheim, Germany) was applied to the corneas to prevent them from drying out. Animals were placed on a heating mat and additionally covered with a tissue paper to avoid hypothermia. Light was delivered from a Lumencor Sola light engine (Beaverton, OR, USA) light source equipped with a light conductor and a custom-made blue light filter (430 nm). Light intensity was measured with a RM-12 radiometer (Opsytec, Ettlingen, Germany) with a VISBG sensor (400 to 570 nm). For illumination, a cover slide was placed on the cornea to eliminate light scatter. Illumination took place with an intensity of 50 mW/cm^2 for 15 min. The non-illuminated eye was shielded from stray light by carefully covering it with aluminium foil. Care was taken so the light beam entered the eye along the optical axis. After light exposure, narcosis was antagonized by s.c. injection of an antidote (naloxone 1•2 mg/kg body weight, flumazenil 0•5 mg/kg body weight, atipamezole 2•5 mg/kg body weight) and animals were kept in a dark room for 7 days before sacrifice. This setup results

in reproducible light damage around the optic nerve head, as corroborated by SLO/OCT and histology (Fang et al., manuscript submitted). Non-illuminated eyes served as control.

2.4. Isolation of RPE and choroidal granules

RPE granules were isolated from human donor eyes (12 eyes, mean age 70•2 years ± 14•7 years standard deviation; range 46 to 91 years) and pig eyes, obtained from a local slaughter house, according to published methods [27]. Choroidal melanosomes were additionally isolated from pig eyes. In brief, eyes were opened close to the ora serrata and the anterior segment and vitreous were discarded. The retina was removed with forceps and the eyecups washed with PBS pH 7•4 (Gibco, Carlsbad, CA, USA). Eyecups were filled with trypsin/EDTA (Gibco, Carlsbad, CA, USA) and incubated for 10 min at 37 °C. RPE cells were washed from Bruch's membrane by repeatedly pipetting the trypsin solution and collected in DMEM supplemented with 10% foetal bovine serum (Gibco, Carlsbad, CA, USA) to stop the enzymatic reaction. Porcine choroid was collected by gently removing it from the sclera with forceps. RPE cells and choroidal tissue were pelleted by centrifugation and homogenized using a tissue grinder. Cell debris was removed by centrifugation for 7 min at 60 g and the obtained supernatant was centrifuged for 10 min at 6000 g to pellet all pigment granules. The pellets were collected in 0·3 M sucrose, loaded on a discontinuous sucrose gradient (2 M to 1 M in 8 steps for human granules [27] and in 2 steps for porcine granules [8]) and centrifuged for 1 h at 103,000 g. Bands containing lipofuscin granules were identified by their yellow-orange tinge and were collected by carefully removing them with a thin pipette. Melanosomes adhered to the centrifugation tube walls and were washed off after removing the sucrose gradient. Isolated granules were washed in PBS and counted with a haemocytometer. Granules were stored at −20 °C until further use.

2.5. Oxidative stress in isolated melanosomes

Isolated porcine melanosomes were suspended in PBS pH 7•4 to yield a final concentration of 30,000 granules/µl. To induce photic stress, melanosome suspensions were illuminated with 45,000 lx white light (measured with a Colormaster 3 F, Gossen, Nuremberg, Germany) delivered by an LED lamp (SunaEco 1500 Ocean Blue XP, Tropic Marin, Wartenberg, Germany). For oxidative stress, melanosomes were incubated with freshly prepared hydrogen peroxide solution (0•3% in PBS, Sigma-Aldrich, St. Louis, MO, USA) in the dark. Incubation times were up to 6 h. Melanosomes incubated in PBS in the dark served as control. Melanosomes were washed twice with demineralized water and prepared for fluorescence or electron microscopy as described below.

2.6. Sample preparation for fluorescence and electron microscopy

Donor and mouse eyes were fixed, embedded in epon resin and sectioned according to standard procedures [28,29]. For fluorescence analysis, post-fixation and staining with heavy metals was omitted. Semi-thin sections (500 nm) were prepared and coverslipped with Dako fluorescent mounting medium. For electron microscopy, ultra-thin sections (70 nm) were collected on formvar-coated slot grids stained with lead citrate and investigated on a Zeiss 900 electron microscope (Zeiss, Jena, Germany). For fluorescence microscopy of isolated granules, the granule suspension was pipetted onto glass slides and let sit to dry at room temperature in the dark. Samples were cover-slipped with Dako fluorescent mounting medium. For electron microscopy, isolated granules were fixed in 2% glutaraldehyde and encased in 3% NuSieve GTG low melting agarose (Lonza, Rockland, ME, USA) and subjected to embedding and sectioning as described above.

2.7. Fluorescence microscopy

Specimens were investigated with a Zeiss Axioplan 2 microscope (Zeiss, Jena, Germany) equipped with a Lumencor Sola SE II NIR (Beaverton, OR, USA) light source and using a x63 objective. Filter sets were a custom made lipofuscin filter set (excitation 370/36 nm, emission 575/15, 400 nm beam splitter) for SW-AF and a commercial Cy7 filter set (excitation 708/75 nm, emission 809/81 nm, 757 nm beam splitter) for NIR-AF, respectively. The lipofuscin filter set is designed to fit the reported excitation and emission maximums for lipofuscin [30]. Binning x2 was applied for all images and acquisition times, as well as microscope and software settings were held constant for any set of samples to allow comparison of fluorescence intensities. If indicated in the figure legends, images with low AF intensities were post-processed with the Auto adjust colours function of the IrfanView software to allow the localization of weak AF signals. This function enhances the contrast by redefining the darkest pixel as pure black and the brightest pixel as pure white in the histogram on a channel-by-channel basis.

2.8. Semi-quantitative analysis of fluorescence intensities

Fluorescence intensities were determined using Fiji software. Regions of interest were determined in fluorescence and BF images using the default threshold, and area and integrated optical density (IOD) of the region of interest were measured. To correct for varied amounts of pigment granules displayed in each image, fluorescence IOD values were normalized to the area of pigment thresholded in corresponding BF images.

2.9. Correlative fluorescence and electron microscopy

To accommodate the requirements of both fluorescence and electron microscopy, ultra-thin sections with a thickness of 150 nm were used. This allows improved detection of fluorophores compared to standard 70 nm ultra-thin sections (as routinely used for electron microscopy), while still being thin enough to allow electron microscopic investigation (as opposed to 500 nm semi-thin sections that would be too thick to be penetrated by the electron beam). Non-osmicated sections were collected on formvar-coated mesh grids. Grids were placed on glass slides in a drop of water, coverslipped, and investigated with light and fluorescence microscopy as described before. Acquisition times had to be prolonged compared to 500 nm thick sections and additionally the auto-contrast function of the camera capture software was used. Signal-to-noise ratio was rather low due to the limited section thickness, so five pictures per channel were averaged using Photoshop CS2. Since sections tend to adhere to the coverslips, grids had to be carefully manipulated off the coverslips with forceps to not destroy the sections. Nevertheless, sections are stressed by being coverslipped and easily damaged, therefore post-staining with uranyl acetate and lead citrate was ultimately omitted, since this often resulted in complete loss of the sections. Grids were air dried and investigated by electron microscopy as described before. The lack of any heavy-metal staining results in low contrast, but melanosomes and lipofuscin granules are still reliably identifiable.

2.10. Energy-dispersive X-ray - scanning transmission electron microscopy analysis

Energy-dispersive X-ray (EDX) analyses were performed on a scanning transmission electron microscope (STEM; Jeol ARM 200F)

equipped with two JEOL EDX detectors at an acceleration voltage of 200 kV. Images were obtained at a size of 512×512 pixels. The obtained elemental maps were 4 × 4 binned using Fiji software.

2.11. Statistical analysis

JMP 13 software (SAS, Cary, NC, USA) was used for statistical analysis. The null hypothesis was that the groups were not statistically different. Dunnett's test, a multiple parametrical test with alpha correction, was used and $p < 0{\bullet}05$ was considered statistically significant.

3. Results

3.1. Differentiating factors between RPE pigment granules in microscopy

In order to be able to investigate the NIR-AF properties of the different RPE pigment types by microscopy, these pigments need to be clearly distinguished from one another. Fig. 1 illustrates how RPE pigments can be identified by light and electron microscopy. In routine transmission electron microscopy, melanin presents as either spherical or spindle-shaped electron-dense structures [31] (Fig. 1a), while lipofuscin either forms evenly shaped granules (for instance in human or monkey RPE [31,32]) or irregularly shaped granules (for instance in *Abca4*$^{-/-}$ mice [29,33], Fig. 1a). Melanolipofuscin is a complex granule that in healthy aged humans consists of a melanin core and a lipofuscin shell or protrusions [31,32], while in *Abca4*$^{-/-}$ mice, several melanosomes can fuse with one lipofuscin granule [29,33] (Fig. 1a). Analytical electron microscopy approaches, such as EDX mapping, can be used to corroborate the identity of the granules based on their elemental composition (Fig. 1b – d). Nitrogen and sulphur serve as markers for melanin, while phosphorus serves as marker for lipofuscin [32].

In this work, we performed all investigations on tissue that was embedded for electron microscopy in epon resin, but heavy metal-staining steps were omitted since they inhibit autofluorescence. The routine staining procedure for light microscopic investigation of epon-embedded sections involves Toluidine blue that yields a medium blue colour in lipofuscin and lets melanosomes appear dark blue to black (Fig. 1e). However, Toluidine blue inhibits autofluorescence as well, preventing NIR-AF investigation in stained sections. Alternatively, melanin can be readily identified in unstained sections by its inherent colour in bright field (BF), while lipofuscin can be identified in the same section by its characteristic SW-AF (Fig. 1e). Therefore, a combination of BF and SW-AF investigation gives similar information concerning melanosome and lipofuscin distribution than Toluidine staining and also allows the investigation of NIR-AF. Moreover, since the SW-AF is confined to the lipofuscin moiety of melanolipofuscin, melanolipofuscin granules in human samples can easily be identified by a gap in a given SW-AF signal that co-localizes with a bright field-identified melanosome (Fig. 1e). However, this does not apply to mouse samples, since their melanolipofuscin is highly irregular in shape and BF contrast. Therefore, distinguishing between true melanolipofuscin on the one hand, and closely situated melanosomes and lipofuscin granules on the other hand, is difficult using only light and fluorescence microscopy in mouse samples.

3.2. NIR-AF intensity in the RPE and choroid increases with age in pigmented WT mice

To investigate whether NIR-AF intensity and distribution change with age, we compared 3-, 12- and 18-month-old WT mice. We found that overall NIR-AF intensity of BF-confirmed melanosomes in the RPE and choroid increases with age (Fig. 2a, b). To allow the identification of areas with NIR-AF in images with low intensity, images were post-processed as described in the methods section. Post-processing revealed that even at 3 months of age and with very weak intensity, NIR-AF signals are present in both RPE and choroid, just as in 18-month-old samples (Fig. 2c, d). Therefore, post-processing is used throughout the manuscript for images with low AF intensities to allow the detection of weak AF signals. In BF images, choroidal cells with brighter granules than neighbouring melanocytes were evident in all age-groups but appeared to increase in number with age (Fig. 2a). These macrophage-like cells were often round and showed higher NIR-AF intensities compared to the surrounding melanocytes in all age-groups (Fig. 2b-d). Electron microscopic investigation of these cells showed that several melanosomes were clustered and surrounded by a common membrane, while this was not the case in typical melanocytes where each melanosome is surrounded by its own membrane (Fig. 2e). Semi-quantitative analysis of total NIR-AF signals derived from RPE and choroid revealed an approx. 3-fold and 9-fold increase in 12-month-old and 18-month-old animals compared to 3-month-old animals, respectively (SI S1). Melanosomes from 12- and 18-month-old animals appear brighter in BF images than those of 3-month-old animals, especially in the choroid (Fig. 2a, SI S1).

3.3. NIR-AF intensity varies between individual melanosomes and can co-localize with WT mice

In the choroid, some melanosomes were prominent in BF images as they appeared darker and larger in size. However, these melanosomes varied considerably in their NIR-AF intensities: while most of them had pronounced NIR-AF, some only showed very weak NIR-AF (SI S2).

At closer inspection of individual RPE melanosomes, we found that in 3-month-old animals, spindle-shaped RPE melanosomes did not show NIR-AF over their whole profile and AF intensities of these granules were very weak compared to neighbouring spherical melanosomes (Fig. 3). In contrast, spherical RPE melanosomes showed inter-granular variability in their NIR-AF intensity; both very weak and very high intensities were observed (Fig. 3). In 18-month-old animals, spindle-shaped melanosomes had mildly higher NIR-AF intensities compared to neighbouring spherical melanosomes. Most spherical melanosomes in this age-group showed a dark margin and a bright centre in BF images; this characteristic in internal morphology was also evident in NIR-AF as the darker margin had higher NIR-AF intensity compared to the brighter granule centre (Fig. 3).

Since it was suggested that lipofuscin contributes to NIR-AF signals [25], we investigated whether this was also evident in histologic sections of WT animals. In 3-month-old animals, lipofuscin, as identified by SW-AF, was scarce and NIR-AF signals from these granules were not evident (Fig. 3). However, in 18-month-old animals, co-localization of NIR- and SW-AF was readily seen, but not present in all granules (Fig. 3). Photoreceptor outer segments also presented SW-AF that increased with age (Fig. 3), probably due to presence of fluorescent bisretinoid precursors [15,34].

3.4. Co-localization of NIR- and SW-AF in the lipofuscin moiety of melanolipofuscin and in lipofuscin in pigmented WT and Abca4$^{-/-}$ mice

We asked the question whether co-localization of NIR- and SW-AF in lipofuscin was a sign of the lipofuscin at hand being a moiety of melanolipofuscin. Since aged WT mice have moderate levels of lipofuscin, we additionally investigated pigmented *Abca4*$^{-/-}$ mice that accumulate high levels of lipofuscin and melanolipofuscin early in life, with the melanolipofuscin appearing as a fusion of melanosomes and irregularly shaped lipofuscin granules [29,33].

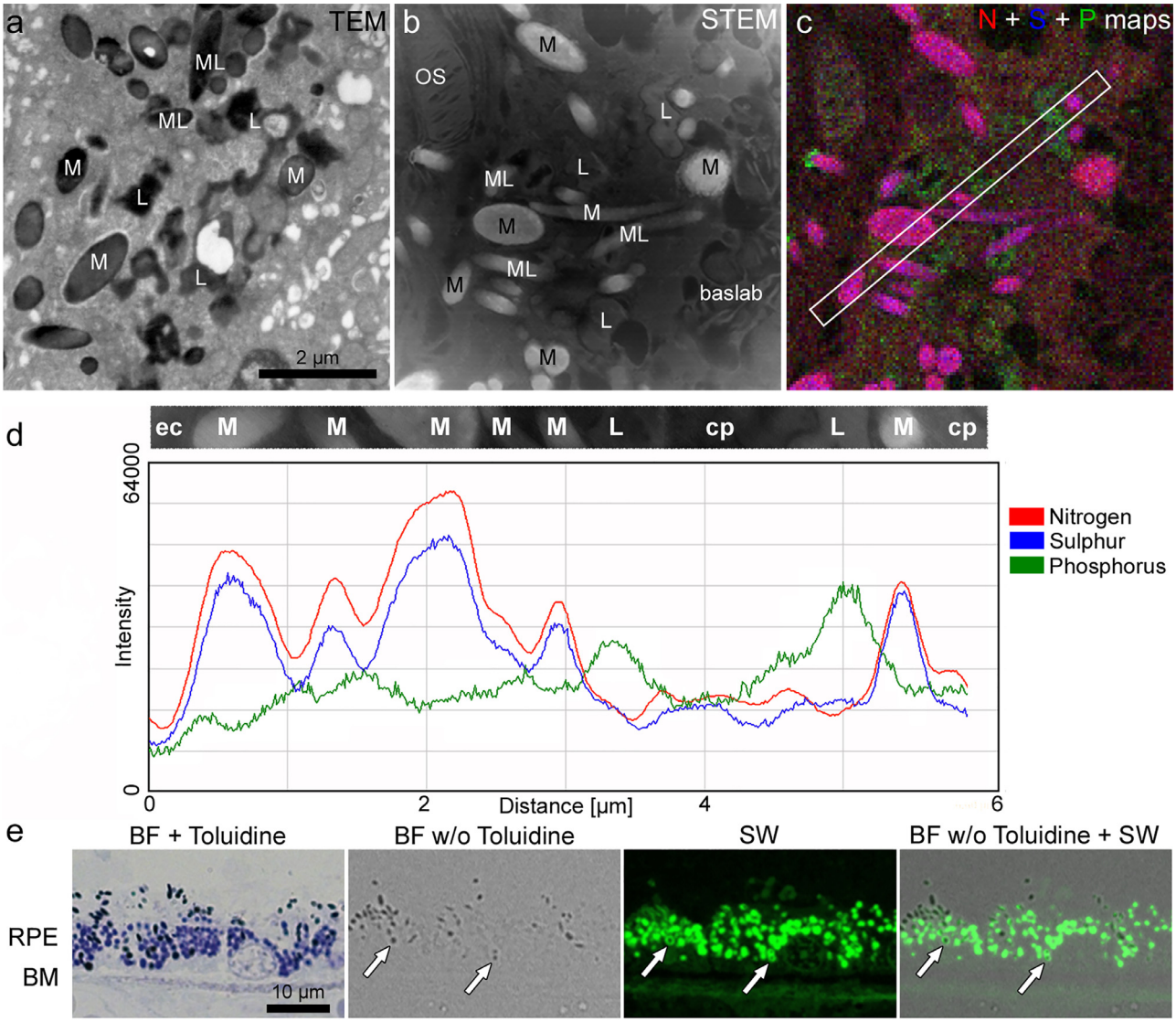

Fig. 1. Distinction between melanosomes, lipofuscin and melanolipofuscin granules in microscopy. a-d) Ultrastructural and elemental identification of pigment granules in an 18-month-old *Abca4*$^{-/-}$ mouse RPE cell. a) Routine transmission electron microscopic image of the RPE showing melanosomes, lipofuscin and melanolipofuscin granules. b) Scanning transmission electron microscopic image of an unstained section of the same eye. c) Superimposition of the 4 × 4 binned EDX maps for nitrogen (N), sulphur (S) (both a marker for melanin) and phosphorus (P) (a marker for lipofuscin) maps of the same area as shown in (b). The box marks a region of interest that crosses several melanosomes and lipofuscin granules. d) Intensity profile of the region of interest shown in (c) highlighting the differing elemental composition of the respective pigment granules. e) Light and fluorescence microscopical identification of RPE pigment granules in a 68-year-old human donor eye. Staining with Toluidine blue yields dark blue to black melanosomes and blue lipofuscin granules. Without Toluidine blue staining, only melanosomes are readily visible in bright field images, however, lipofuscin can be identified in the same section by its characteristic SW-AF. Since SW-AF is confined to the lipofuscin moiety of melanolipofuscin, also regularly shaped melanolipofuscin granules can be identified (arrows). baslab: basal labyrinth; BF: bright field; BM: Bruch's membrane; cp: cytoplasm; ec: extra cellular; M: melanosome; ML: melanolipofuscin; L: lipofuscin; OS: outer segment; RPE: retinal pigment epithelium; STEM: scanning transmission electron microscopy; TEM: transmission electron microscope; SW: short wavelength.

While in 18-month-old WT mice, co-localization of NIR- and SW-AF was exclusively seen adjacent to BF verified melanosomes, 13-month-old *Abca4*$^{-/-}$ mice, with higher lipofuscin levels showed co-localization of NIR- and SW-AF additionally in granules that were spatially separated from melanosomes (Fig. 4). This suggests that in these animals, also lipofuscin granules can emit NIR-AF.

When comparing young (7 months) to aged (13 months) pigmented *Abca4*$^{-/-}$ mice, an overall increase of the NIR-AF signal and brightening of melanosomes in BF images, the latter predominantly in the choroid, similar to the results in WT mice, was evident (SI S3).

Furthermore, in 7-month-old *Abca4*$^{-/-}$ mice, NIR-AF derived from lipofuscin granules was rare, resulting in predominantly green lipofuscin granules in NIR-AF/SW-AF overlay images as opposed to the majority of lipofuscin granules in 13-month-old *Abca4*$^{-/-}$ mice that appeared yellow in NIR-AF/SW-AF overlay images (Fig. 4, SI S3). This suggests that, in these animals, lipofuscin granules can also emit NIR-AF (Fig. 4, SI S3).

3.5. *Lipofuscin in albino* Abca4$^{-/-}$ *mice does not show specific NIR-AF signals*

Histologic differences between lipofuscin from pigmented and albino *Abca4*$^{-/-}$ mice were described before [29]. Furthermore, RPE cells of pigmented and albino *Abca4*$^{-/-}$ mice show varying SW-AF patterns which might be due to the differences in lipofuscin morphology [29]. Therefore, we compared NIR-AF properties of 12–13 months old pigmented and albino *Abca4*$^{-/-}$ mice to age-matched

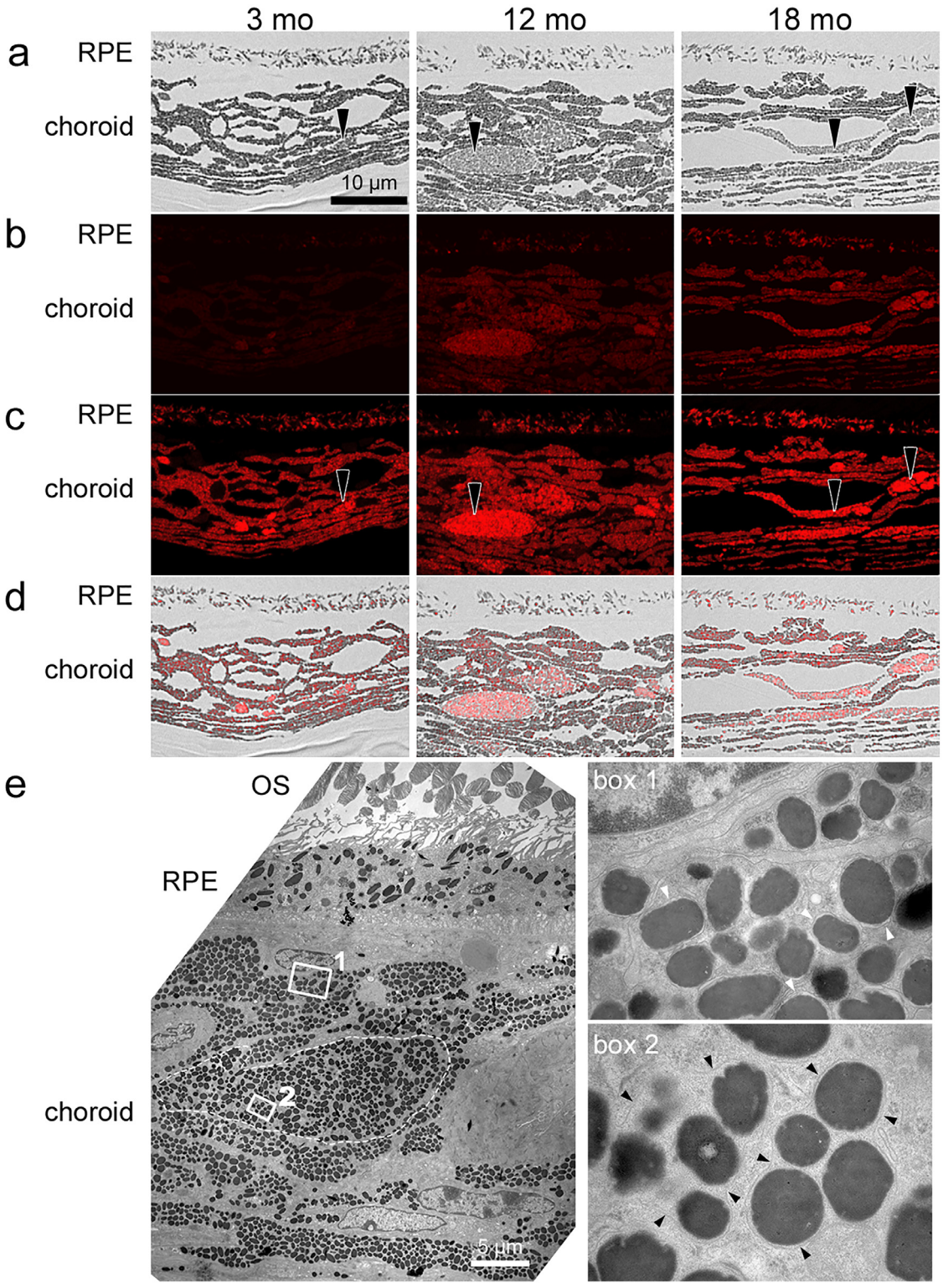

Fig. 2. NIR-AF in the RPE and choroid increases with age in pigmented WT mice. a) BF images of samples from 3-, 12- and 18-month-old mice. Since staining with toluidine blue would have resulted in loss of AF signal, only melanosomes can be identified. Arrowheads point to choroidal cells with brighter granules than typical choroidal melanocytes. b) Corresponding NIR-AF images taken under identical conditions. c) Same images as shown in (b), but post-processed to allow the localization of weak signals. Arrowheads show that choroidal cells with bright granules (as shown in (a)) have a higher NIR-AF intensity compared to the surrounding melanocytes, independent of age. d) Overlay of BF (a) and post-processed NIR-AF (c) images. $N = 1–2$ animals/group. e) Electron microscopic image of a macrophage-like cell (marked with a dashed line) in a 12-month-old pigmented WT mouse. The boxed areas of a typical melanocyte and the macrophage-like cell are shown in higher magnification on the right side. In choroidal melanocytes, individual melanosomes are surrounded by their respective membranes that are in close contact to the granule in young animals, but are often detached in aged animals (box 1, white arrowheads). In macrophage-like cells, several melanosomes form clusters that are surrounded by a continuous membrane (box 2, black arrowheads). OS: outer segments; RPE: retinal pigment epithelium.

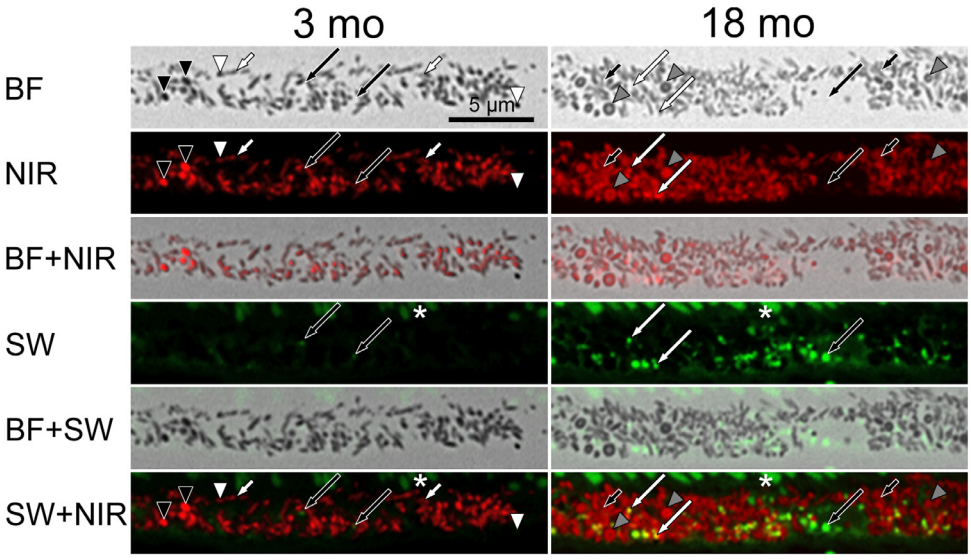

Fig. 3. RPE melanosomes vary in their NIR-AF properties and lipofuscin granules can add to the total NIR-AF signal. Comparison of NIR-AF (red) and SW-AF (green) in 3 and 18-month-old WT mice. AF images were post-processed to allow the localization of weak signals. In young mice, most spindle-shaped melanosomes show weak NIR-AF (short white arrows), while in old mice, most spindle-shaped melanosomes show strong NIR-AF (short black arrows) relative to neighbouring spherical melanosomes. Spherical, dark melanosomes vary between weak NIR-AF (white arrowheads) and very intense NIR-AF (black arrowheads). In old animals, spherical melanosomes with dark margin were evident in BF (grey arrowheads). The dark margin had higher NIR-AF intensity than the bright centre. Areas with high SW-AF sometimes also showed additional NIR-AF (overlay of red and green, yielding yellow; long white arrows), while in other instances and in young animals did not (long black arrows). Asterisks mark autofluorescent outer segments. $N = 1–2$ animals/group. BF: bright field; NIR: near-infrared; SW: short wavelength.

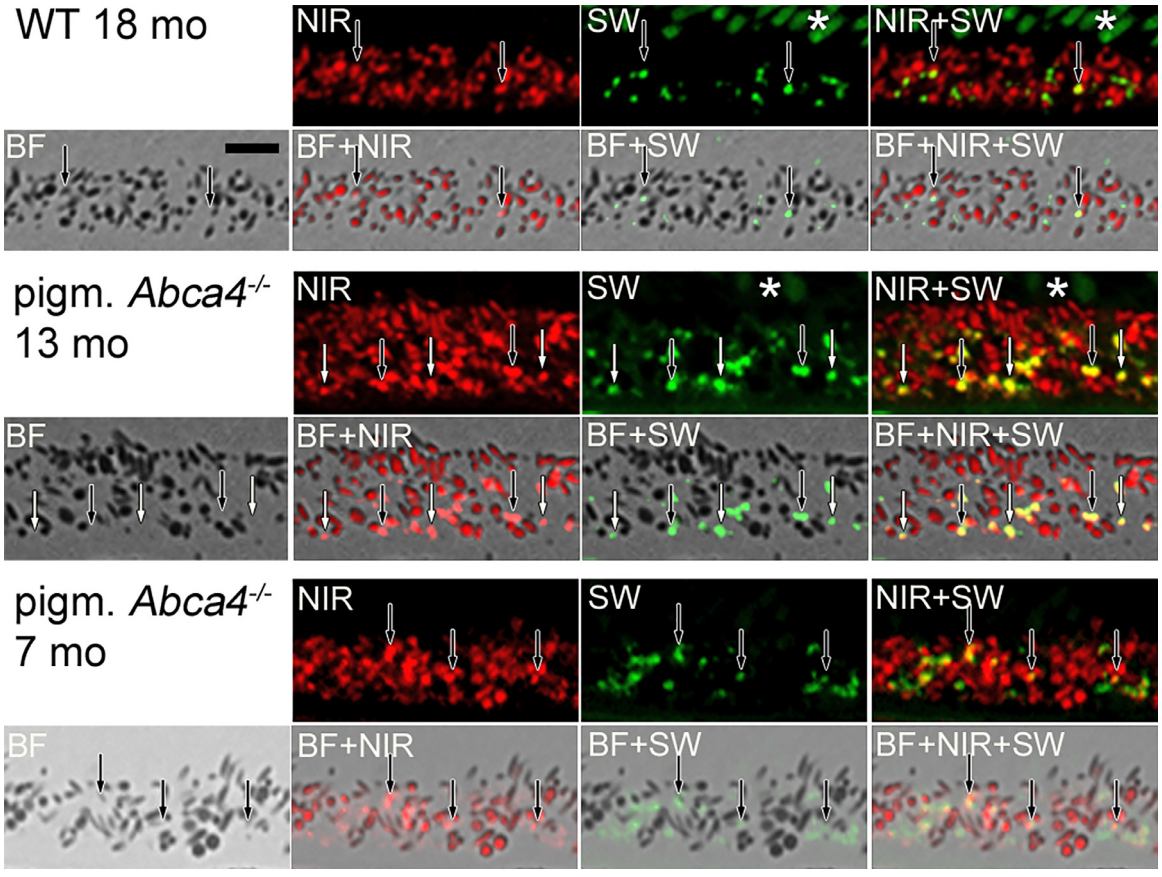

Fig. 4. Co-localization of NIR-AF and SW-AF in the RPE of WT and pigmented *Abca4*$^{-/-}$ mice. NIR-AF is shown in red while SW-AF is shown in green, yielding yellow when superimposed. Black arrows point to co-localization of NIR-AF and SW-AF in direct contact to BF-identified melanosomes, while white arrows point to co-localization of NIR-AF and SW-AF spatially separated from melanosomes. Asterisks mark autofluorescent outer segments. Scale bar: 2 µm. $N = 1–2$ animals per group. BF: bright field; NIR: near-infrared; SW: short wavelength.

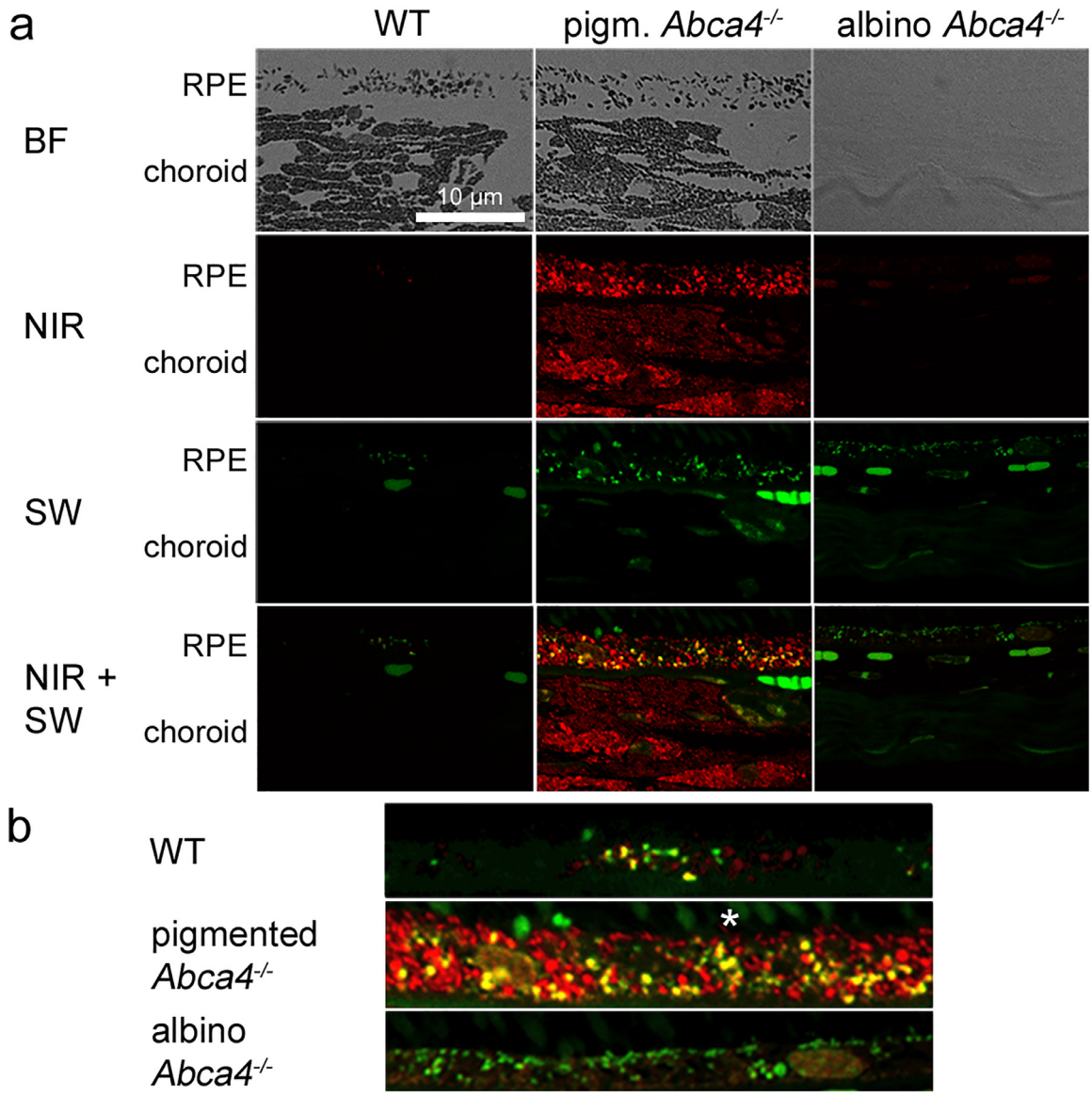

Fig. 5. Comparison of NIR-AF and SW-AF in 12 to 13 months old WT and pigmented and albino *Abca4*$^{-/-}$ mice. NIR-AF (red) and SW-AF (green) images of the different strains were taken under identical conditions. Yellow colour shows areas where NIR-AF and SW-AF superimpose. a) Overview of RPE and choroidal BF, NIR-AF and SW-AF. Note that there are no tissue structures visible in the BF image of the albino mouse, due to lack of melanin and lack of additional staining. AF Images are not post-processed to allow comparison of AF intensities. b) Magnified overlay of NIR-AF and SW-AF images of the RPE areas shown in (a). AF Images are post-processed to allow the localization of weak signals. An asterisk marks autofluorescent outer segments. $N = 1–2$ animals per group. BF: bright field; NIR: near-infrared; SW: short wavelength.

pigmented WT. In pigmented *Abca4*$^{-/-}$ mice, melanosomes of the RPE and choroid gave higher NIR-AF signals than in age-matched WT mice (Fig. 5a). In albino *Abca4*$^{-/-}$ mice, choroidal and RPE melanosomes are lacking and consequently no melanosome-derived NIR-AF signals were found.

Correlation of NIR- and SW-AF showed that in WT mice, some, but not all lipofuscin granules present NIR-AF (Fig. 5b). In pigmented *Abca4*$^{-/-}$ mice, most areas with SW-AF also showed NIR-AF (Fig. 5b), independent of whether they were in close contact to BF-identified melanosomes or being spatially separate from melanosomes. Only very small lipofuscin granules did not exhibit NIR-AF. In albino *Abca4*$^{-/-}$ mice however, no specific NIR-AF signals co-localizing with SW-AF were present (Fig. 5b). When we used prolonged acquisition times, very weak NIR-AF signals co-localizing with SW-AF were found in albino *Abca4*$^{-/-}$ mice, however, the signal intensity was comparable to background signal (SI S4).

3.6. NIR- AF signals in aged human RPE originate from melanosomes, melanolipofuscin and lipofuscin granules

To verify the findings from mouse tissue, we investigated tissue of two aged human donors (68 and 80 years) without known ophthalmic diseases. Virtually all of the SW-AF co-localized with NIR-AF, some of it being in direct contact to BF-identified melanosomes, suggesting melanolipofuscin (SI S5). Melanosomes and lipofuscin granules show similar intensity of NIR-AF and the NIR-AF signal is present in the whole lipofuscin granule profile, resulting in a bright yellow colour in the overlay image. Lipofuscin granules showing SW-AF, but not NIR-AF, were scarce and small in diameter. Routine electron microscopy confirmed overall localization and morphology of granules identified by fluorescence microscopy; just as in fluorescence images, melanolipofuscin consisted of a melanin core with a shell or protrusions of lipofuscin-

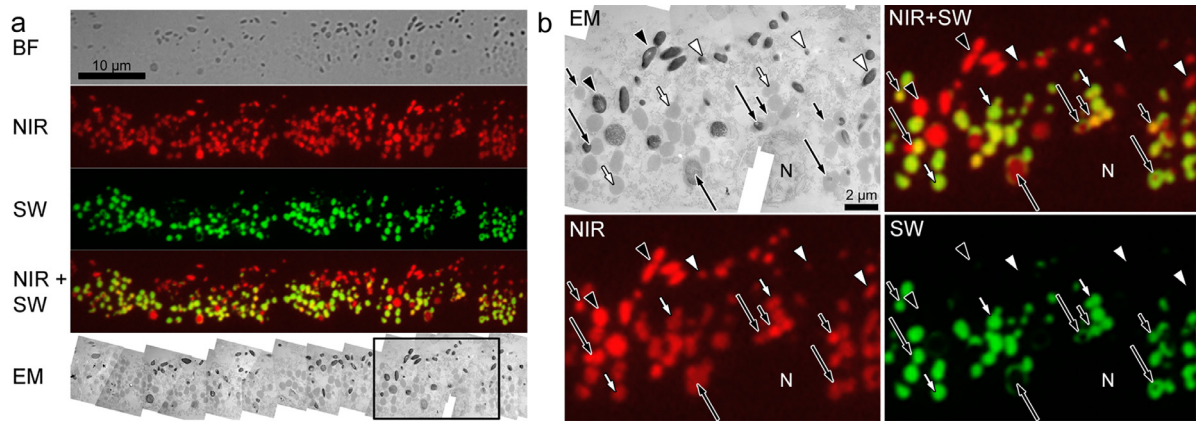

Fig. 6. Correlative fluorescence and electron microscopy of the RPE of an 80-year-old human donor. a) A 150 nm thick section was first investigated by BF and for NIR-AF (red) and SW-AF (green) and subsequently investigated by electron microscopy. To compensate for low signal to noise ratio, 5 individual images of BF, NIR-AF and SW-AF were averaged, respectively. In the NIR-/SW-AF overlay image, lipofuscin granules appear yellow due to the presence of both NIR- and SW-AF. The EM image shown is a composite image of 20 individual images taken at x12,000 magnification. Contrast is low due to complete lack of heavy-metal staining, however, melanosomes and (melano-)lipofuscin granules are still readily identifiable (compare to SI S5 that shows a heavy-metal stained section from the same eye). Magnified EM and fluorescence pictures of the boxed area are shown in (b). The full resolution version of the EM composite image can be accessed under DOI:10.6084/m9.figshare.7951097. b) Melanosomes (arrowheads) show exclusively NIR-AF, but no SW-AF. However, NIR-AF intensity varies between high (black arrowheads) and low (white arrowheads). Lipofuscin granules (short arrows) appear ultrastructurally indistinguishable and show similar SW-AF intensities, but their NIR-AF intensities vary between high (short black arrows) and low (short white arrows). Virtually all lipofuscin granules present NIR-AF. Melanolipofuscin granules (long arrows) can be identified by their NIR-AF positive melanin core and a SW-AF and NIR-AF positive lipofuscin shell or protrusions. BF: bright field; EM: electron microscopy; N: nucleus; NIR: near-infrared; SW: short wavelength.

like material (SI S5). Lipofuscin granules had typical spherical morphology with a homogenous electron-opaque matrix (SI S5).

To corroborate that aged human lipofuscin has both NIR- and SW-AF, we investigated isolated human RPE granules that were separated by density gradient centrifugation into lipofuscin, melanolipofuscin and melanosome fractions (SI S6). In the lipofuscin fraction most granules showed both NIR- and SW-AF. Few granules showed only NIR-AF, but no SW-AF, pointing to minor contamination with melanosomes, as confirmed by electron microscopy. Granules showing only SW-AF, but no NIR-AF, were not present.

In a final step, we performed correlative fluorescence and electron microscopy on single tissue sections. For this, 150 nm thick sections were first investigated by fluorescence microscopy and the same sections were then examined by transmission electron microscopy. This allows unequivocal attribution of fluorescence signals to individual granules within the RPE. Fig. 6 shows that virtually all lipofuscin granules identified by EM showed both SW-AF and NIR-AF. Melanolipofuscin granules are clearly identified by their NIR-AF presenting melanin core and a shell or protrusions of lipofuscin that is positive for both SW- and NIR-AF. Melanosomes varied in their NIR-AF intensity (Fig. 6), but never showed SW-AF.

3.7. *Photic and oxidative stress intensify NIR-AF of melanosomes* in vitro

Since both light and oxidative stress have been found to increase melanin AF [10–12], we tested whether these stressors also increase NIR-AF of melanosomes. Therefore, isolated RPE and choroidal melanosomes from pig eyes were treated with either white light (45,000 lx) or 0•3% hydrogen peroxide at pH 7•4 for 3 or 6 h, respectively (Fig. 7, SI S7). NIR-AF intensity from RPE melanosomes increased significantly after 6 h of light treatment and already after 3 h of hydrogen peroxide treatment, respectively. For choroidal melanosomes, significant alterations of NIR-AF were only seen after 6 h of hydrogen peroxide treatment and not after the applied illumination conditions. Brightening was especially seen in choroidal melanosomes (SI S7). SW-AF was not found in either melanosome fraction in any of the investigated conditions. Ultrastructural analysis of control and treated granules found that light treated RPE melanosomes showed an increase in number and size of small holes close to the melanosome edge, whereas hydrogen peroxide treatment resulted in a less homogenous electron density of RPE melanosomes (SI S8). In choroidal melanosomes, ultrastructural changes were less obvious.

3.8. *NIR-AF of both melanosomes and lipofuscin granules increase in an* in vivo *phototoxicity model*

The pigmented *Abca4*$^{-/-}$ mouse strain is considered as a model for the early phase of Stargardt disease, since it mimics the accumulation of lipofuscin in the RPE but lacks the retinal degeneration encountered in Stargardt patients. Illumination with blue light can be used to induce retinal degeneration which can be considered as a model for the late stage of Stargardt disease. We used a slightly modified phototoxicity protocol based on that published by Wu et al. [26] (Fang et al., manuscript submitted).

We found that the NIR-AF intensity and the share of the melanosome profiles that exhibit NIR-AF in the RPE and to a lesser extent in the choroid increases after illumination of 9-month-old *Abca4*$^{-/-}$ mice (Fig. 8). Furthermore, also the share of lipofuscin granules with co-localizing SW- and NIR-AF increases. These findings resemble the previously described data from aged WT and pigmented *Abca4*$^{-/-}$ mice (Figs. 2–4, SI S3).

4. Discussion

Light exposure of melanin is known to result in extensive structural modifications such as oxidative cleavage and cross-linking [7]. Photodegradation of DHICA-melanin, a synthetic model for eumelanin that is the major melanin type in the eye, resulted in a 16-fold increase of AF intensity [9].

In the present work, we show that NIR-AF emerging from RPE and choroidal melanosomes increases with age (Figs. 2, 3, SI S3) and oxidative stress (Figs. 7, SI S7). Additionally, NIR-AF emerging from RPE melanosomes increases with light stress as well (Figs. 7, 8, S7). Furthermore, while melanosomes in the RPE and choroid of 12-month-old WT mice have very low NIR-AF intensity, melanosome-derived NIR-AF signals from age-matched pigmented *Abca4*$^{-/-}$ mice are greatly increased (Fig. 5). This might be due to

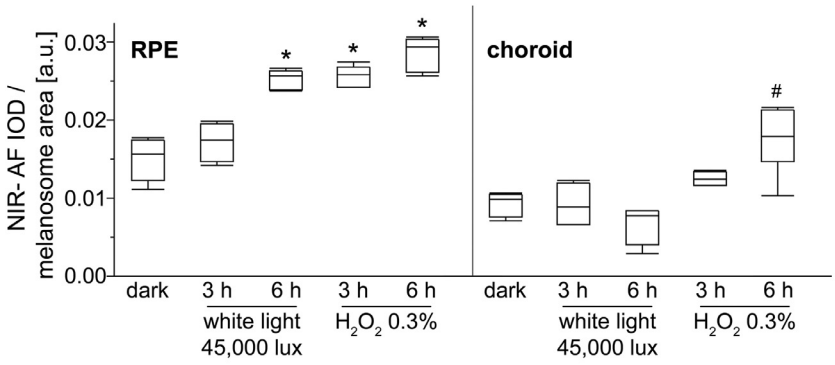

Fig. 7. Semi-quantitative analysis of NIR-AF intensities of RPE and choroidal melanosomes after photic and oxidative stress. Isolated porcine RPE and choroidal melanosomes were treated with either 45,000 lx white light or 0·3% hydrogen peroxide at pH 7•4 for 3 or 6 h, respectively ($N = 4$–6, # $p < 0$•01, * $p < 0$•0001, Dunnett's test). IOD: integrated optical density; NIR: near-infrared.

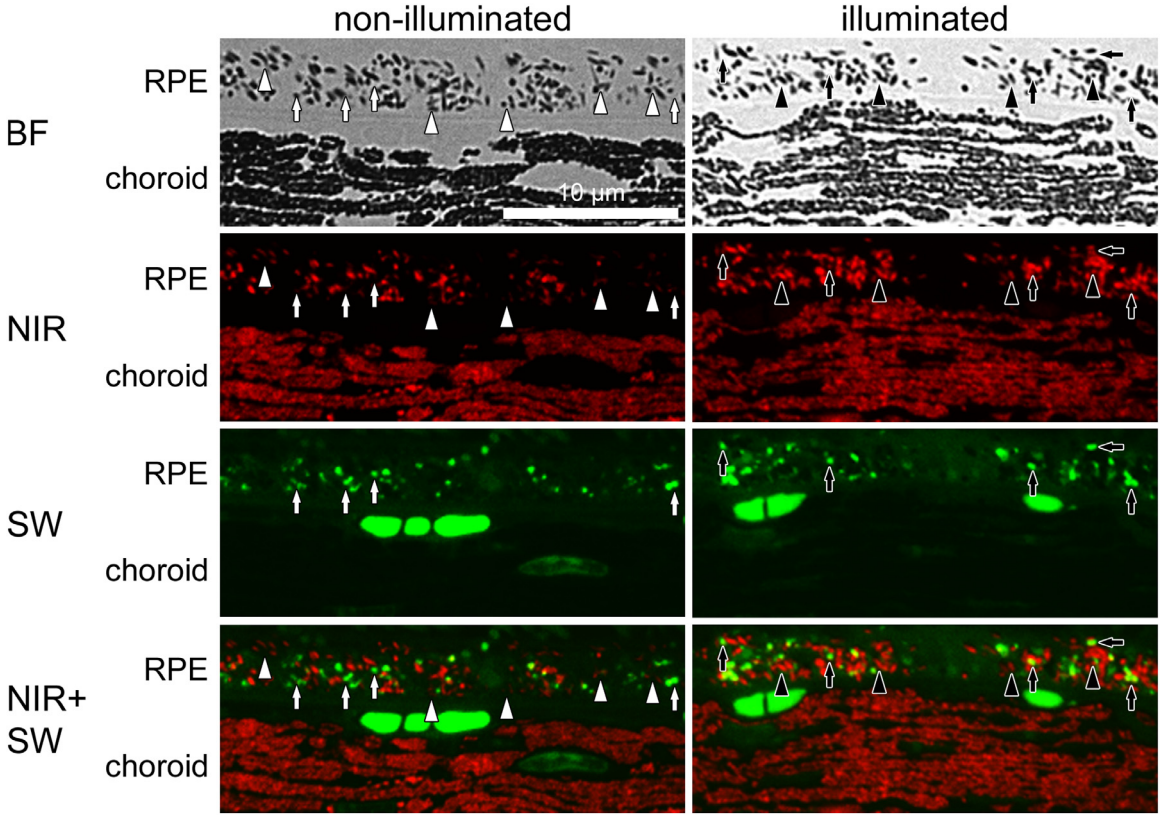

Fig. 8. Blue light stress increases NIR-AF signals in 9-month-old pigmented *Abca4*$^{-/-}$ mice. NIR-AF (red) and SW-AF (green) images of both groups were taken under identical conditions. In non-illuminated eyes, many melanosomes show only minimal or no NIR-AF (white arrowheads), while after blue light stress the overall number of melanosomes showing NIR-AF and the NIR-AF intensity increases (black arrowheads). In non-illuminated eyes, the majority of lipofuscin granules only show SW-AF (white arrows), while after illumination the number of lipofuscin granules showing co-localization of SW-AF and NIR-AF increases (black arrows). $N = 7$ animals per group. BF: bright field; NIR: near-infrared; SW: short wavelength.

melanin damage caused by elevated levels of oxidative stress in these animals. These findings question the common assumption that NIR-AF is an intrinsic property of melanin; it may be more appropriate to consider NIR-AF as a marker for aged or oxidized melanin.

In addition to an increase of NIR-AF intensity with age, we saw a simultaneous brightening of melanosomes in BF images in WT and *Abca4*$^{-/-}$ mice, especially in the choroid (Fig. 2, SI S1, SI S3). Melanosome bleaching is most likely due to melanin degradation, as bleaching also occurs after treatment with superoxide anions, known to degrade melanin [13]. This suggests that the observed increase of NIR-AF is linked to melanin degradation.

Melanosomes from RPE and choroidal melanocytes differ in their reaction to photic and oxidative damage: while RPE melanosomes exhibit more readily NIR-AF (Fig. 7), choroidal melanosomes react more readily with granule brightening (SI S7). Both melanosome types consist mostly of eumelanin with only little amounts of pheomelanin, however, choroidal melanin is suggested to have a higher 5,6-dihydroxyindole-2-carboxylic acid (DHICA) to 5,6-dihydroxyindole (DHI) ratio, with DHICA and DHI being the two proposed monomers of eumelanin [35]. A high DHICA:DHI ratio was suggested to be indicative of a high potential to quench reactive oxygen species [36]. This difference in chemical composition might at least partly explain the observed dif-

ference in reaction to photic and oxidative damage in RPE and choroidal melanosomes (Fig. 7, SI S7, SI S8). Acknowledging the different properties of RPE and choroidal melanin is of interest for fundus AF, since with current clinical imaging systems, both RPE and choroidal melanin add to the NIR-AF measurements [19,20]. However, new imaging techniques, such as adaptive optics scanning laser ophthalmoscopy, are being developed that allow the selective visualisation of RPE cells [37].

Furthermore, we found that there is a considerable variation in NIR-AF properties within both the RPE and the choroidal melanosome populations. In young RPE cells, ellipsoidal melanosomes have a uniform weak NIR-AF that does not cover the whole melanosome profile, whereas spherical melanosomes show a high inter-granule variability, with either very high or very low NIR-AF intensity (Fig. 3). In the choroid, melanosomes that seem uniform in light microscopy can differ vastly in their NIR-AF intensity (SI S2). It seemed that this variability was more prominent in 18-month-old animals, however, this might be due to overall weak NIR-AF intensities in young animals making it difficult to detect such variabilities in these specimens. Little is known about potential functional differences between ellipsoidal and spherical melanosomes of the RPE, however, both types of RPE melanosomes do not differ in their melanin composition, they mostly contain eumelanin. For choroidal melanosomes, even less is known about their function and properties. The inter-granule difference in NIR-AF intensities in a given tissue is a sign that individual melanosomes are not subjected to the same levels of noxious agents that can induce chemical alterations which finally result in NIR-AF intensity increase.

In the choroid, individual rounded cells were present that showed elevated NIR-AF intensities compared to the neighbouring, typically elongated melanocytes (Fig. 2, SI S2). Ultrastructural investigation revealed clusters of melanosomes in lysosome-like organelles in these cells (Fig. 2E). Our group previously identified choroidal cells with similar morphology as macrophages by immunohistochemistry [38].

The contribution of lipofuscin to the NIR-AF signal has long been under debate [25,39]. We found the first occurrences of co-localization of SW- and NIR-AF in areas adjacent to BF-identified melanosomes, suggesting that the lipofuscin moiety of melanolipofuscin is the first area to present both AF types (Figs. 3, 4, SI S3). With increased load of lipofuscin, also lipofuscin granules (indicated by spatial separation from BF-identified melanosomes) did readily contribute to the NIR-AF signal, although the proportion of NIR-AF-contributing lipofuscin granules varies (Figs. 3–6, SI S3, S5). When investigating isolated human RPE granules, the lipofuscin fraction showed both SW- and NIR-AF (SI S6). The possibility of misidentifying melanolipofuscin as lipofuscin granules, *e.g.* due to the melanin moiety not being visible in the section, was prevented by separating the granules by density centrifugation and investigating whole granules.

To our surprise, we did not detect specific lipofuscin NIR-AF signals from albino *Abca4*$^{-/-}$ mice (Fig. 5). With longer acquisition times, we found weak NIR-AF signals co-localizing with lipofuscin granules with high SW-AF intensities, however, these NIR-AF signals were merely as intense as background signals derived from nuclei (SI S4). We therefore suppose that these signals are fluorescence spillover from lipofuscin fluorophores and are not derived from the same molecular source as the high-intensity NIR-AF signals found in lipofuscin granules from pigmented animals and aged humans. So while lipofuscin in albino *Abca4*$^{-/-}$ mice lacks the high-intensity NIR-AF signal seen in pigmented samples, some NIR-AF background is present. This is in accordance with the results from a fundus AF-based study by Paavo et al. that found an increase of NIR-AF intensities in tandem with SW-AF intensities in albino *Abca4*$^{-/-}$ mice[25]: our data suggest that increasing amounts of lipofuscin result in increasing SW-AF and a mild parallel increase of NIR-AF due to presumed fluorescence spillover in these animals. Lipofuscin from pigmented and albino mice was shown to have different bisretinoid composition [40] and morphological properties [29], therefore a difference in NIR-AF properties due to molecular differences is conceivable. In histologic sections and isolated granules from aged human donors however, virtually all lipofuscin granules (and lipofuscin moieties of melanolipofuscin granules) exhibited co-localization of SW- and NIR-AF (Fig. 6, SI S5, SI S6).

How can we explain these observed differences in lipofuscin NIR-AF intensities? As outlined before, co-localization of SW- and NIR-AF first emerging in close association to bright-field-confirmed melanosomes is suggestive of the granule in question being melanolipofuscin. This suggests that the lipofuscin moiety in melanolipofuscin has certain properties that distinguish it from true lipofuscin granules. Analytical electron microscopy as well as nano-secondary ion mass spectrometry analyses of human RPE pigments found that the lipofuscin moiety of melanolipofuscin has significantly elevated nitrogen levels (usually considered a marker for protein content, but also a marker for melanin) compared to lipofuscin granules, while the melanin moiety of melanolipofuscin was found to have elevated phosphorus levels (considered a marker for lipid content) compared to true melanosomes [28,32]. This suggests that the lipofuscin and melanin moieties in melanolipofuscin have some sort of molecular exchange. It is possible that the elevated nitrogen levels found in melanolipofuscin are in fact not derived from proteins, but from melanin degradation products that also contain nitrogen atoms.

Assuming that melanin degradation products amass in melanolipofuscin, how can we explain their subsequent presence in lipofuscin granules? Melanosomes and lipofuscin granules - and consequently melanolipofuscin granules as well - are part of the lysosomal compartment [5,15]. It was shown that lysosomes can exchange contents [41] and it was hypothesized that this occurs by similar mechanisms, as they are established for lysosome-endosome exchange [42]. Moreover, lipofuscin granule dynamics and linkage to degradative processes of melanosomes have been suggested before [31]. To our knowledge, potential trafficking processes between RPE pigments have not been investigated to date. However, it was shown that phagocytosed material, including material associated to phagocytosed outer segments, is transported to melanosomes [43,44] which highly suggests an involvement of the melanosome in the lysosomal degradation pathway. By this means, bisretinoids are likely to be transported to the melanosome. Due to their oxidative properties, bisretinoids might therefore be involved in melanin degradation. Additionally, this process might be the gateway to melanolipofuscin formation. Indeed, we previously suggested the hypothesis that melanosomes can degrade ingested bisretinoids by radical processes and that an insufficient degradation of these ingested bisretinoids results in their accumulation within the melanosome, yielding melanolipofuscin (Schraermeyer U, et al. Invest Ophthalmol Vis Sci. 2019;60:ARVO E-Abstract 1912). The concept of melanin being able to degrade bisretinoids is supported by recent findings highlighting that human foetal RPE cells accumulate less lipofuscin-like material than unpigmented RPE cells *in vitro* [45]. Little is known about the biological fate of melanin degradation products. It is conceivable that fluorescent degradation products of melanin are incorporated into the lipofuscin moiety of melanolipofuscin granules and, with time, are distributed to lipofuscin granules by mechanisms similar to lysosome-lysosome exchange mechanisms. This would not only explain the increase of lipofuscin granules with co-localized SW- and NIR-AF with time, but also elegantly explain the observed lack of specific high-intensity NIR-AF, exceeding what we currently consider fluores-

cence spillover, in albino *Abca4*$^{-/-}$ lipofuscin. Furthermore, accumulation of melanin-degradation products in lipofuscin granules with time could also lead to a tipping point when lipofuscin granules have a greater contribution to overall NIR-AF than melanosomes, especially considering that melanosomes are lost from the RPE with age.

However, molecular confirmation of melanin degradation products accumulating in (melano-)lipofuscin is currently lacking. To date, most compositional analyses of lipofuscin are based on extracts obtained by Folch extraction, which only allows the investigation of chloroform-soluble lipids, therefore, new analytic approaches, going beyond Folch extraction, are needed.

A potential weakness of this study is that we had to resort to standard fluorescence microscopy, since even though the confocal laser scanning system at our disposal (Leica TCS SP8 STED) is equipped with multiple excitation lasers, excitation with 708 nm or longer is not available. We tested whether 635 nm (the longest excitation wavelength available in our system) can be used for excitation of NIR-AF but this resulted in no detectable signals from both melanosomes and lipofuscin granules in a range from 648 to 800 nm, as detected with a Leica prism-based tuneable multiband spectral detection system. However, since we limited section thickness to 500 nm, we were still able to achieve good resolution in standard fluorescence microscopy. Furthermore, *Abca4*$^{-/-}$ and WT mice belong to different substrains of the 129S strain, so we cannot rule out the presence of genetic differences that influence the presented results between these two mouse models. Another limitation is the low number of biological replicates. Nevertheless, the increase of melanin-derived NIR-AF with oxidative and photic stress was found in melanosomes from two species (mouse and pig) as was the presence of NIR-AF signals in lipofuscin (mouse and human). We therefore consider our results a proof-of-concept that requires further investigation. One important question is for instance the degree of influence increasing melanin-derived NIR-AF and additionally occurring lipofuscin-derived NIR-AF have on patient fundus autofluorescence data. Also the underlying mechanism and time frame of lipofuscin granules emitting NIR-AF is of high relevance as is its potential involvement in lipofuscin-related retinal disease, such as in age-related macular degeneration and Stargardt disease.

Strengths of this study are that the used NIR excitation and emission wavelengths are very similar to the wavelengths used in fundus AF examination in patients, so the NIR-AF findings in this study are transferable to patient findings. Furthermore, the microscopical approach employed allows identification of AF properties of individual granules, which is not yet possible with clinical fundus AF based techniques. However, new techniques, such as adaptive optics scanning laser ophthalmoscopy, have the potential to achieve subcellular resolution *in vivo* in the future [37]. Correlative fluorescence and electron microscopy showed unambiguously that both melanosomes and lipofuscin granules are sources of NIR-AF in aged human donor eyes.

In conclusion, our study suggests that NIR-AF is derived from melanin degradation products that emerge from either photic or oxidative stress. As a consequence, aged/damaged melanosomes emit higher NIR-AF signals than young/undamaged melanosomes. Therefore, melanin could be considered a “wear and tear” material that is meant to quench photic or oxidative stress at its own expense. This is indicated by elevated NIR-AF levels in the RPE and choroid of pigmented *Abca4*$^{-/-}$ mice that have more oxidative stress than age-matched WT mice. Pigmented *Abca4*$^{-/-}$ mice do not develop retinal degeneration even up to 22 months of age, while albino *Abca4*$^{-/-}$ mice show first signs of retinal damages as early as 4 months old [29]. Although pigmented and albino *Abca4*$^{-/-}$ mice differ in their genetic background (as discussed in [29]), the lack of melanin in the RPE and choroid of albino *Abca4*$^{-/-}$ mice can at least partly explain the differing susceptibility to retinal degeneration.

However, also the lipofuscin moiety of melanolipofuscin and subsequently lipofuscin granules can emit relevant levels of NIR-AF, potentially due to accumulation of melanin degradation products. The exact mechanism of how and when lipofuscin granules start to emit NIR-AF is however still unclear.

Both aspects, melanin NIR-AF increasing with age and oxidative status, as well as lipofuscin being a source of NIR-AF under certain circumstances, are of great importance for interpretation of clinical and research NIR-AF data. The common assumption that NIR-AF intensity equates melanin quantity cannot be supported with the present data. Elucidating the mechanisms behind changing AF properties of melanosomes and lipofuscin granules opens the possibility to gain deeper insights into pathologic processes and refinement of diagnostics.

5. Funding sources

This work was funded by a grant from Bundesministerium für Bildung und Forschung (01GQ1422B). YF was funded by a Chinese Scholarship Council. AB was funded by Deutsche Forschungsgemeinschaft (BI1551/3-1). The laser scanning microscope was funded by a grant from Deutsche Forschungsgemeinschaft (INST 2388/62-1). The STEM-EDX system was supported by funds of the European Fund for Regional Development (EFRE-FKZ: 712303), the state of Baden-Württemberg, and the NMI Reutlingen. The funders were not involved in study design, data collection, data analysis, data interpretation, decision to publish, or manuscript writing.

6. Declaration of Competing Interest

The authors declare that they have no competing interests.

7. Author contributions

Conceptualization: TT, SJS, US; Data curation: TT; Formal analysis: TT; Funding acquisition: US; Investigation: TT, YF, AB; Supervision: SJS, US; Visualization: TT; Writing - original draft: TT; Writing - review and editing: YF, AB, SJS, US

Acknowledgments

The authors thank Peter Charbel Issa, Gabriel H. Travis, and Roxana Radu for providing them with the knockout mouse strains. They also thank the Cornea Bank Tübingen for providing them with human eye tissue. Special thanks are due to the donors and their families. The authors also thank Timm Schubert for performing the confocal laser scanning microscopy analysis and Sigrid Schultheiss, Barbara Illing, and Antonina Burda for excellent technical assistance. We also thank Clementine Warres and Max Becker for their support in STEM handling.

Supplementary materials

Supplementary material associated with this article can be found, in the online version, at doi:10.1016/j.ebiom.2019.09.048.

References

[1] Hu DN, Simon JD, Sarna T. Role of ocular melanin in ophthalmic physiology and pathology. Photochem Photobiol 2008;84:639–44.
[2] Dontsov AE, Glickman RD, Ostrovsky MA. Retinal pigment epithelium pigment granules stimulate the photo-oxidation of unsaturated fatty acids. Free Radic Biol Med 1999;26:1436–46.

[3] Biesemeier A, Kokkinou D, Julien S, et al. UV-A induced oxidative stress is more prominent in naturally pigmented aged human RPE cells compared to non-pigmented human RPE cells independent of zinc treatment. J Photochem Photobio B Bio 2008;90:113–20.
[4] Rozanowski B, Cuenco J, Davies S, et al. The phototoxicity of aged human retinal melanosomes. Photochem Photobiol 2008;84:650–7.
[5] Schraermeyer U, Heimann K. Current understanding on the role of retinal pigment epithelium and its pigmentation. Pigment Cell Res 1999;12:219–36.
[6] Poliakov E, Strunnikova NV, Jiang JK, et al. Multiple A2E treatments lead to melanization of rod outer segment-challenged ARPE-19 cells. Mol Vis 2014;20:285–300.
[7] Ito S, Wakamatsu K, Sarna T. Photodegradation of eumelanin and pheomelanin and its pathophysiological implications. Photochem Photobiol 2018;94:409–20.
[8] Zareba M, Szewczyk G, Sarna T, et al. Effects of photodegradation on the physical and antioxidant properties of melanosomes isolated from retinal pigment epithelium. Photochem Photobiol 2006;82:1024–9.
[9] Wakamatsu K, Nakanishi Y, Miyazaki N, Kolbe L, Ito S. UVA-induced oxidative degradation of melanins: fission of indole moiety in eumelanin and conversion to benzothiazole moiety in pheomelanin. Pigment Cell Melanoma Res 2012;25:434–45.
[10] Elleder M, Borovansky J. Autofluorescence of melanins induced by ultraviolet radiation and near ultraviolet light. A histochemical and biochemical study. Histochem J 2001;33:273–81.
[11] Kayatz P, Thumann G, Luther TT, et al. Oxidation causes melanin fluorescence. Invest Ophthalmol Vis Sci 2001;42:241–6.
[12] Sarna T, Burke JM, Korytowski W, et al. Loss of melanin from human RPE with aging: possible role of melanin photooxidation. Exp Eye Res 2003;76:89–98.
[13] Dontsov AE, Sakina NL, Ostrovsky MA. Loss of melanin by eye retinal pigment epithelium cells is associated with its oxidative destruction in melanolipofuscin granules. Biochem Biokhimiia 2017;82:916–24.
[14] Docchio F, Boulton M, Cubeddu R, Ramponi R, Barker PD. Age-related changes in the fluorescence of melanin and lipofuscin granules of the retinal pigment epithelium: a time-resolved fluorescence spectroscopy study. Photochem Photobiol 1991;54:247–53.
[15] Sparrow JR, Gregory-Roberts E, Yamamoto K, et al. The bisretinoids of retinal pigment epithelium. Prog Retin Eye Res 2012;31:121–35.
[16] Ach T, Huisingh C, McGwin G Jr, et al. Quantitative autofluorescence and cell density maps of the human retinal pigment epithelium. Invest Ophthalmol Vis Sci 2014;55:4832–41.
[17] Schmitz-Valckenberg S, Holz FG, Bird AC, Spaide RF. Fundus autofluorescence imaging: review and perspectives. Retina 2008;28:385–409.
[18] Yung M, Klufas MA, Sarraf D. Clinical applications of fundus autofluorescence in retinal disease. Int J Retina Vitreous 2016;2:12.
[19] Keilhauer CN, Delori FC. Near-infrared autofluorescence imaging of the fundus: visualization of ocular melanin. Invest Ophthalmol Vis Sci 2006;47:3556–64.
[20] Weinberger AW, Lappas A, Kirschkamp T, et al. Fundus near infrared fluorescence correlates with fundus near infrared reflectance. Invest Ophthalmol Vis Sci 2006;47:3098–108.
[21] Pilotto E, Vujosevic S, Melis R, et al. Short wavelength fundus autofluorescence *versus* near-infrared fundus autofluorescence, with microperimetric correspondence, in patients with geographic atrophy due to age-related macular degeneration. Br J Ophthalmol 2011;95:1140–4.
[22] Cideciyan AV, Swider M, Schwartz SB, Stone EM, Jacobson SG. Predicting progression of ABCA4-Associated retinal degenerations based on longitudinal measurements of the leading disease front. Invest Ophthalmol Vis Sci 2015;56:5946–55.
[23] Duncker T, Tabacaru MR, Lee W, Tsang SH, Sparrow JR, Greenstein VC. Comparison of near-infrared and short-wavelength autofluorescence in retinitis pigmentosa. Invest Ophthalmol Vis Sci 2013;54:585–91.
[24] Skondra D, Papakostas TD, Hunter R, Vavvas DG. Near infrared autofluorescence imaging of retinal diseases. Semin Ophthalmol 2012;27:202–8.
[25] Paavo M, Zhao J, Kim HJ, et al. Mutations in GPR143/OA1 and ABCA4 inform interpretations of short-wavelength and near-infrared fundus autofluorescence. Invest Ophthalmol Vis Sci 2018;59:2459–69.
[26] Wu L, Ueda K, Nagasaki T, Sparrow JR. Light damage in Abca4 and Rpe65rd12 mice. Invest Ophthalmol Vis Sci 2014;55:1910–18.
[27] Boulton M, Marshall J. Repigmentation of human retinal pigment epithelial cells *in vitro*. Exp Eye Res 1985;41:209–18.
[28] Biesemeier A, Eibl O, Eswara S, Audinot JN, Wirtz T, Schraermeyer U. Transition metals and trace elements in the retinal pigment epithelium and choroid: correlative ultrastructural and chemical analysis by analytical electron microscopy and nano-secondary ion mass spectrometry. Metallomics 2018;10:296–308.
[29] Taubitz T, Tschulakow AV, Tikhonovich M, et al. Ultrastructural alterations in the retinal pigment epithelium and photoreceptors of a Stargardt patient and three Stargardt mouse models: indication for the central role of RPE melanin in oxidative stress. PeerJ 2018;6:e5215.
[30] Jung T. Hohn a and grune T. lipofuscin: detection and quantification by microscopic techniques. Methods Mol Biol 2010;594:173–93.
[31] Feeney L. Lipofuscin and melanin of human retinal pigment epithelium. Fluorescence, enzyme cytochemical, and ultrastructural studies. Invest Ophthalmol Vis Sci 1978;17:583–600.
[32] Biesemeier A, Schraermeyer U, Eibl O. Chemical composition of melanosomes, lipofuscin and melanolipofuscin granules of human RPE tissues. Exp Eye Res 2011;93:29–39.
[33] Charbel Issa P, Barnard AR, Singh MS, et al. Fundus autofluorescence in the Abca4(-/-) mouse model of Stargardt disease–correlation with accumulation of A2E, retinal function, and histology. Invest Ophthalmol Vis Sci 2013;54:5602–12.
[34] Paavo M, Lee W, Allikmets R, Tsang S, Sparrow JR. Photoreceptor cells as a source of fundus autofluorescence in recessive Stargardt disease. J Neurosci Res 2019;97:98–106.
[35] Liu Y, Hong L, Wakamatsu K, et al. Comparisons of the structural and chemical properties of melanosomes isolated from retinal pigment epithelium, iris and choroid of newborn and mature bovine eyes. Photochem Photobiol 2005;81:510–16.
[36] Sarangarajan R, Apte SP. Melanin aggregation and polymerization: possible implications in age-related macular degeneration. Ophthalmic Res 2005;37:136–41.
[37] Granger CE, Yang Q, Song H, et al. Human retinal pigment epithelium: in vivo cell morphometry, multispectral autofluorescence, and relationship to cone mosaic. Invest Ophthalmol Vis Sci 2018;59:5705–16.
[38] Julien S, Biesemeier A, Kokkinou D, Eibl O, Schraermeyer U. Zinc deficiency leads to lipofuscin accumulation in the retinal pigment epithelium of pigmented rats. PLoS ONE 2011;6:e29245.
[39] Gibbs D, Cideciyan AV, Jacobson SG, Williams DS. Retinal pigment epithelium defects in humans and mice with mutations in MYO7A: imaging melanosome-specific autofluorescence. Invest Ophthalmol Vis Sci 2009;50:4386–93.
[40] Ueda K, Zhao J, Kim HJ, Sparrow JR. Photodegradation of retinal bisretinoids in mouse models and implications for macular degeneration. Proc Natl Acad Sci USA 2016;113:6904–9.
[41] Ferris AL, Brown JC, Park RD, Storrie B. Chinese hamster ovary cell lysosomes rapidly exchange contents. J Cell Biol 1987;105:2703–12.
[42] Storrie B, Desjardins M. The biogenesis of lysosomes: is it a kiss and run, continuous fusion and fission process. Bioessays 1996;18:895–903.
[43] Schraermeyer U, Stieve H. A newly discovered pathway of melanin formation in cultured retinal pigment epithelium of cattle. Cell Tissue Res 1994;276:273–9.
[44] Schraermeyer U, Peters S, Thumann G, Kociok N, Heimann K. Melanin granules of retinal pigment epithelium are connected with the lysosomal degradation pathway. Exp Eye Res 1999;68:237–45.
[45] Zhang Q, Presswalla F, Calton M, et al. Highly differentiated human fetal RPE cultures are resistant to the accumulation and toxicity of lipofuscin-like material. Invest Ophthalmol Vis Sci 2019;60:3468–79.